Geophysical Research Letters

RESEARCH LETTER
10.1029/2023GL105568

The Stability Transition From Stable to Unstable Frictional Slip With Finite Pore Pressure

R. Affinito[1], C. Wood[1], S. Marty[1], D. Elsworth[1,2], and C. Marone[1,3]

[1]Department of Geosciences, Pennsylvania State University, University Park, PA, USA, [2]Department of Energy and Mineral Engineering, EMS Energy Institute, G3 Center, Pennsylvania State University, University Park, PA, USA, [3]Dipartimento di Scienze della Terra, La Sapienza Università di Roma, Rome, Italy

Key Points:

- The frictional stability transition does not require dilatant hardening for granular fault zones sheared at low pore pressures
- Slow earthquakes and quasi-dynamic fault slip can be explained by the strain-rate dependence of the critical fault stiffness (Kc)
- For the effective normal stresses studied, pore pressure has a negligible impact on frictional stability and the mode of fault slip

Supporting Information:

Supporting Information may be found in the online version of this article.

Correspondence to:

R. Affinito,
affinito@psu.edu

Citation:

Affinito, R., Wood, C., Marty, S., Elsworth, D., & Marone, C. (2024). The stability transition from stable to unstable frictional slip with finite pore pressure. *Geophysical Research Letters*, *51*, e2023GL105568. https://doi.org/10.1029/2023GL105568

Received 19 JUL 2023
Accepted 4 DEC 2023

Author Contributions:

Conceptualization: D. Elsworth
Data curation: C. Wood
Formal analysis: C. Wood, C. Marone
Funding acquisition: C. Marone
Resources: C. Marone
Supervision: C. Marone
Writing – review & editing: C. Wood, S. Marty, D. Elsworth, C. Marone

Abstract Pore fluids are ubiquitous throughout the lithosphere and are commonly invoked as the cause of induced seismicity and slow earthquakes. We perform lab experiments to address these questions for drained fault conditions and low pore pressure. We shear simulated faults at effective normal stress (σ_n') of 20 MPa and pore pressures P_p from 1 to 4 MPa. We document the full range of lab earthquake behaviors from slow slip to elasto-dynamic rupture and show that slow slip can be explained by the slip rate dependence of the critical rheologic stiffness without dilatancy hardening or other fluid effects. Our fault permeabilities ranges from 10^{-18} to 10^{-17} m^2 with an initial porosity of 0.1 and estimated fluid diffusion time ≈1 s. Slow slip and quasi-dynamic fault motion may arise from high P_p at higher pressures but dilatancy strengthening is not a general requirement.

Plain Language Summary Earthquakes begin and propagate within the fluid-saturated rocks of Earth's crust. Many investigators have suggested that high pore fluid pressure (Pp) is essential for slow earthquakes and tremor. These studies rely on the idea that changes in Pp can impact rupture propagation speed by dilatant volume increase during faulting with concurrent increases in fault effective normal stress. Thus, understanding the processes that produce slow-slip versus dynamically propagating rupture is integral to seismic hazard forecasting. Here, we describe experiments on granular faults that produce the full spectrum of slip observed in nature. We measure the mechanical and hydraulic behavior of the faults and determine that frictional and fluid-driven processes occur in conjunction. Importantly, we demonstrate that frictional processes are sufficient to explain slow-slip when fluid migration is not inhibited. We demonstrate that for low pore fluid pressures, the full transition from slow slip to dynamic rupture events can be explained as a frictional effect via the critical rheologic stiffness.

1. Introduction

Slow earthquakes, tremor, and other quasi-dynamic modes of fault slip (collectively: slow slip events SSE) are considered to be analogs of ordinary, elastodynamic earthquakes (Dal Zilio et al., 2020). SSE are observed in many settings, yet the mechanisms that dictate rupture propagation speed in these cases remain poorly understood. In many cases, SSE occur at depths associated with metamorphic dehydration (Behr & Bürgmann, 2021) where alterations in permeable pathways are associated with elevated pore pressure (Williams, 2019). Elevated pore pressure are therefore commonly suggested as the cause of SSE (Condit & French, 2022). Indeed, laboratory studies have shown that fracturing and fault slip can induce pore volume changes that effectively strengthen the fault (Brantut, 2020). These observations are consistent with mechanisms such as seismic pumping, fault-valve behavior (Sibson, 1986), and dilational strengthening (Segall et al., 2010). However, SSE occur in a wide range of settings. Moreover, it is unclear whether dynamic fluid responses act to stabilize fault slip or destabilize via mechanisms such as thermal pressurization (Segall & Rice, 2006). The details of slip-induced volume changes and fault permeability are essential to resolve these questions, but are thus far only poorly constrained. Here, we address these issues with laboratory friction experiments under finite pore pressure conditions.

The Coulomb frictional theory proposes that high pore pressure reduces fault strength, bringing it closer to failure (Ellsworth, 2013; Hubbert & Rubey, 1959). However, while the Coulomb-Mohr failure criterion predicts the stress state, it does not address the stability of frictional motion, and whether seismic or aseismic slip occurs. In fact, a reduction in effective normal stress, on its own, tends to produce stable frictional sliding. The role of fluids in

tectonic faulting is clearly important but the wide range of conditions under which SSE occur (Bürgmann, 2018; Sacks et al., 1978) suggests that other mechanisms are important.

Pore fluid pressures and fluid pathways are highly variable along the subducting interface (Behr & Bürgmann, 2021). Understanding whether pore fluid pressure fluctuations are the result of modulations in the effective normal stress or due to dissipation via fluid diffusion (Faulkner & Rutter, 2001) could provide insight into the driving mechanisms behind pore fluid pressure evolution and SSE along the subducting interface. Dilational strengthening requires an increase in pore volume via slip that results in a reduction of the pore fluid pressure, which temporarily increases the effective stress across the fault. The opposite can also occur whereby undrained compaction leads to increased P_p and weakening via fluid pressurization (Segall et al., 2010). Numerical models suggest that anisotropic permeability associated with pore pressure pulses may be the primary control on SSEs in systems such as Hikurangi or Cascadia (Perez-Silva et al., 2023). Such mechanisms are often invoked, however, few studies of SSEs analogs from the lab exist to test these ideas.

Experimental studies on fracture of intact samples show that dilatancy can stabilize slip events (Aben & Brantut, 2021). Moreover, measurements of volumetric changes in experimental faults (Aben & Brantut, 2021; Brantut, 2020; Ji et al., 2022; Marone et al., 1990; Proctor et al., 2020; Samuelson et al., 2009) highlight the importance of the drainage state on fluid pressure responses by illustrating that the dilatancy rate with fault slip can lead to dilatancy hardening. Yet, only a few studies have successfully measured fault zone storage (Wibberley, 2002), as fault zone thickness varies greatly during slip events (Rice, 2006). These data sets are critical for characterizing the role of dilational processes on slip.

Laboratory studies have documented slow and quasi-dynamic slip (Leeman et al., 2016) along with the full range of slip modes from aseismic creep to dynamic rupture. Complex modes of fault slip occur when the loading stiffness K is nearly equal to the critical frictional weakening rate (or rheological stiffness) K_c (Gu et al., 1984). The rheological stiffness, $K_c = (\sigma_n - P_p)\,(b-a)/D_c$, where $(\sigma_n - P_p)$ is the effective normal stress, $(b-a)$ defines the frictional rate dependence and D_c is the critical slip distance, as described in the rate and state constitutive framework (RSF) (Dieterich, 1979; Gu et al., 1984; Marone, 1998; Ruina, 1983). Within the framework of RSF, we expect fluid pressure to influence the mode of slip and the transition from stable creep to stick-slip events (lab earthquakes). Extensive studies have demonstrated the frictional transition in the absence of fluid pressures (Leeman et al., 2015, 2016; Scuderi et al., 2016, 2017; Shreedharan et al., 2020). However, few studies have documented the stability transition for fluid saturated conditions. Here, we present such data with specific focus on the fault drainage state, which is vital to address the fluid-driven mechanism often invoked for slow-slip. We describe laboratory work to investigate slow-slip and the frictional stability transition under constant fluid pressure boundary conditions. Here we describe lab work investing slow-slip and the frictional stability transition under constant fluid pressure boundary conditions. Our lab data are available to everyone (Affinito et al., 2023).

2. Experimental Methods

Our experiments were conducted in a true-triaxial pressure vessel (Figure 1a), using the double direct shear (DDS) configuration (Ikari et al., 2009; Kenigsberg et al., 2020; Samuelson et al., 2009). We used a synthetic fault gouge composed of quartz powder (Min-U-Sil 40) with a median grain size of 10.5 μm. Two uniform layers were constructed using a leveling jig to achieve a reproducible initial thickness of 3 mm. The layers were each 5.7 cm × 5.4 cm in area. For simplicity, we reference all stresses, strains, and displacements to a single fault layer of the DDS arrangement. Total shear displacements ranged from 22 to 25 mm, corresponding to shear strain between 20 and 26. Samples were sealed in a flexible latex jacket to separate confining and pore pressures (see Text S1 in Supporting Information S1; Figure 1c).

Normal stress (σ_n) and shear stress (τ) are applied and maintained via servo-controlled hydraulic rams (Figure 1a). Upstream and downstream pore fluid pressures (P_p) and confining pressure (P_c) were independently servo-controlled. For our sample geometry (see Text S1 in Supporting Information S1; Figure 1c) fault normal stress is given by $\sigma_n + P_c$, for a Terzhagi effective normal stress, $\sigma_n' = \sigma_n + P_c - P_p$. As such, the pore fluid ratio λ can be defined as P_p/σ_n'.

P_p is servo-controlled at a constant value and we measure both upstream and downstream volume fluxes to determine fault perpendicular permeability. τ on the fault is applied by advancing the central forcing block of the DDS arrangement at a constant displacement rate. Both normal and shear loads are measured by beryllium copper load

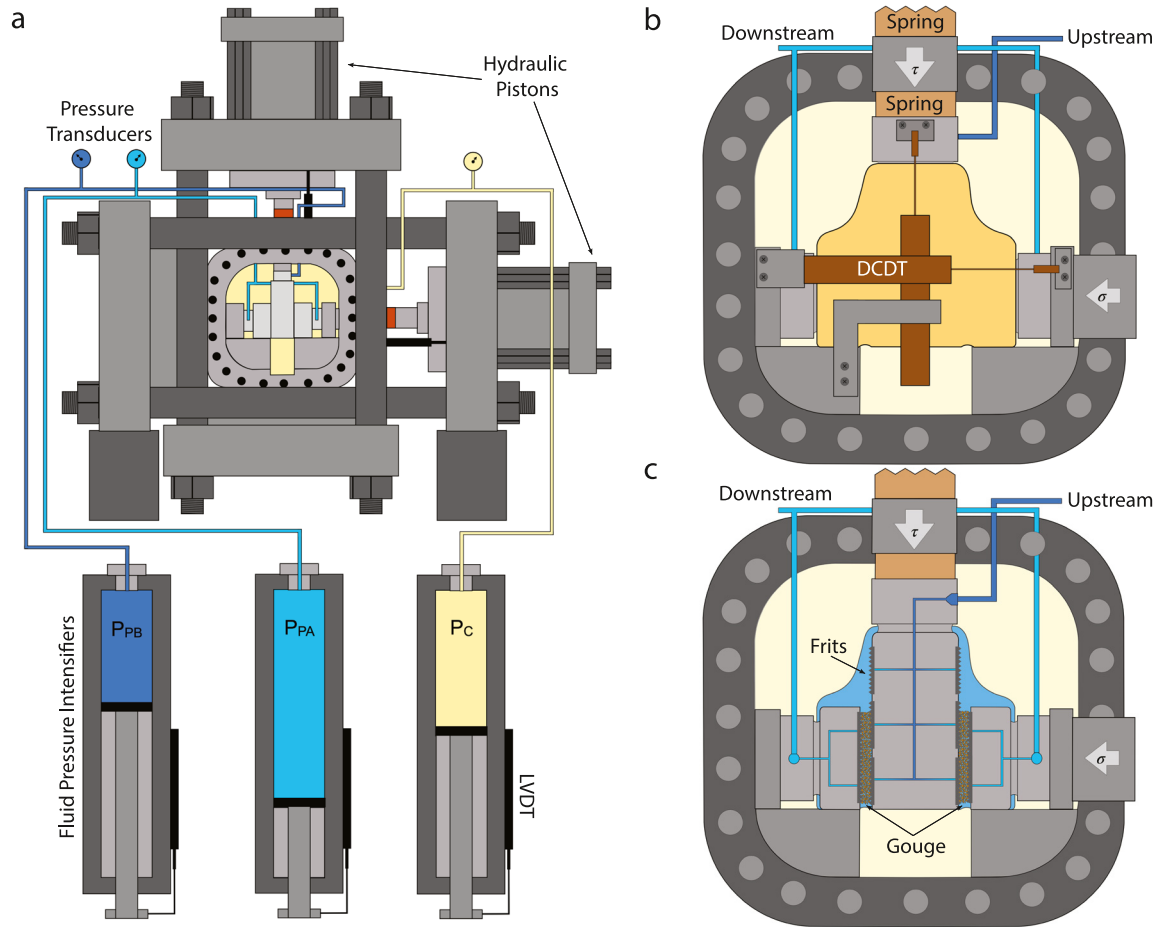

Figure 1. Schematic of the biaxial deformation apparatus and pressure vessel for true triaxial loading. (a) Two hydraulic rams apply normal and shear loads to the steel double direct shear (DDS) sample. Fluid intensifiers control P_c and both upstream and downstream P_p. (b) Internal DCDTs measure fault shear and normal displacements. Springs are placed in series with the vertical loading column to dictate the loading stiffness. (c) We measured fault normal permeability by flowing from the central block to the side blocks of the DDS arrangement. Pore fluids enter the fault via porous sintered metal platens (Mott Corp.).

cells with a precision of 5 N (Figure 1a). Fault shear and normal displacements are measured with direct-current displacement transducers (DCDTs) external to the pressure vessel and in a few cases with DCDTs internal to the vessel; in all cases, the resolution is ±0.1 μm (Figure 1b).

Samples were sheared with pore fluid pressures between 1 and 4 MPa at 10 μm/s, under constant fluid pressure boundary conditions. Pore fluid of de-ionized and deaerated water was delivered to the faults via sintered porous steel platens (see Text S1 in Supporting Information S1; Figure 1b). The platens are serrated with saw-tooth faces to ensure coupling to the gouge layer. P_p was monitored using pressure transducers external to the pressure vessel (Figure 1a) with 0.007 MPa resolution. Loads and displacements were recorded continuously at 10 kHz sampling rates and averaged for storage from 1 Hz to 1 kHz, depending on the shear rate.

2.1. Sample Preparation

The faults are sealed with a composite latex rubber membrane to isolate P_c from P_p. The seal consisted of three layers to prevent puncture during shear: (a) a 3.2 mm thick latex rubber sheet wrapped around the lower part of the sample, (b) a 0.9 mm thick latex rubber tube, and (c) a 1.5 mm thick dip-molded latex jacket for the DDS configuration (Figure 1c).

2.2. Reduction of Apparatus Loading Stiffness

Our goal is to study the transition from stable to unstable sliding, thus we reduced the shear loading stiffness K to match the fault rheological stiffness K_c. Loading stiffness was reduced using two acrylic rods (springs) 42 mm in

diameter and 35 mm in length in the shear loading column. One rod was outside the vessel at the load point and the other was inside the pressure vessel between the piston and the sample (Figure 1c). Loading stiffness calibration experiments showed that P_c has an effect on the spring stiffness, thus confining pressure was held constant (see Figure S1 in Supporting Information S1).

2.3. Permeability and Fault Zone Strain

We measured fault permeability and its evolution with strain in experiments with a special loading history. Permeability was measured every 5 mm of shear displacement with the following protocol. (a) The vertical piston was locked in place. (b) A constant P_p boundary condition was imposed between the upstream (PpA) and downstream (PpB) (Figure 1a). (c) Flow normal to the fault was sustained until steady-state rates were achieved. The across-fault permeability was calculated using Darcy's law:

$$k = \frac{Q\mu L}{A\Delta P} \quad (1)$$

Steady-state flow was ensured by measuring upstream and downstream volume flux, where Q is the fluid discharge, μ is the dynamic viscosity of water at room temperature (24°C), L is the fault layer thickness (accounting for layer compaction/dilation), A is the sample cross-sectional area, and ΔP is the pore pressure differential. Upstream and downstream values of Q differing by <10% were considered steady-state (see Text S1 and Figure S9 in Supporting Information S1).

2.4. Experimental Procedure

Experiments began by applying σ_n of 3 MPa, followed by 2 MPa P_c, after which P_p was increased to 1 MPa. Samples were saturated by (a) bleeding air from pressure lines and (b) imposing a 0.5 MPa P_p differential across the sample to atmosphere. When constant fluid flow was achieved, (c) P_p was increased to 1 MPa, and the bleed valve was closed. At this point, upstream and downstream P_p values were equalized, followed by a final check for trapped air.

After saturation, σ_n was increased to the target stress (18–21 MPa) and P_c was increased to 5 MPa. During this compaction stage, P_p was increased to the target value (1–4 MPa). Experiments began with a permeability measurement, after compaction, followed by a 10 μm/s shear loading segment with a shear unload/reload stage at 3 and 6 mm to promote comminution and steady-state shear fabric (Figure 3a). We sheared samples for up to 25 mm, and then locked the vertical piston and made a final permeability measurement (Figure 1b) before unloading.

3. Results

Stress-displacement curves for our experiments show a linear shear stress increase followed by gradual yield (Figure 2). After the shear unload/cycles we observe a period of stable sliding followed by emergent, quasi-periodic unstable slow-slip (Figure 2a). The slip events are laboratory analogs of earthquakes, which are often referred to as "labquakes." The initial labquakes are slow and complex with irregular stress drop and slip velocity. Eventually they transition to a regular recurrence interval, interpreted as a limit cycle indicating steady-state conditions for labquakes. This steady-state is dictated friction, fault zone shear fabric (via the fault rheological stiffness, K_c) and by the loading stiffness, K. Samples typically reached peak friction at shear strains ranging from 7 to 9. We found that fault slip transitioned from stable to quasi-unstable motion at shear strains of 10–12. The unstable slip events begin as small-amplitude oscillations that grow over 10–20 slip cycles (Figure 2b).

The initial fault thickness ranged from 2.8 to 3.2 mm. Initial compaction during shear loading ranged from 0.8 to 1 mm, followed by 0.4–0.5 mm of thinning during shearing. Fault zone porosity ranged from 8% to 12% after compaction. A separate suite of experiments were used to measure permeability evolution as a function of strain. Permeability evolved from 10^{-18} to 10^{-17} m^2 (see Figures S2 and S9 in Supporting Information S1), with the greatest decrease occurring from 0 to 10 shear strain. Once the fault reached steady-state friction, permeability reduction was minor (see Figure S2 in Supporting Information S1).

3.1. Lab Earthquake Measurements

For each slip event, we measured the co-seismic and inter-seismic periods using the maximum and minimum shear stress to define the beginning and end of failure (Figure 2c, see Figure S4 in Supporting Information S1).

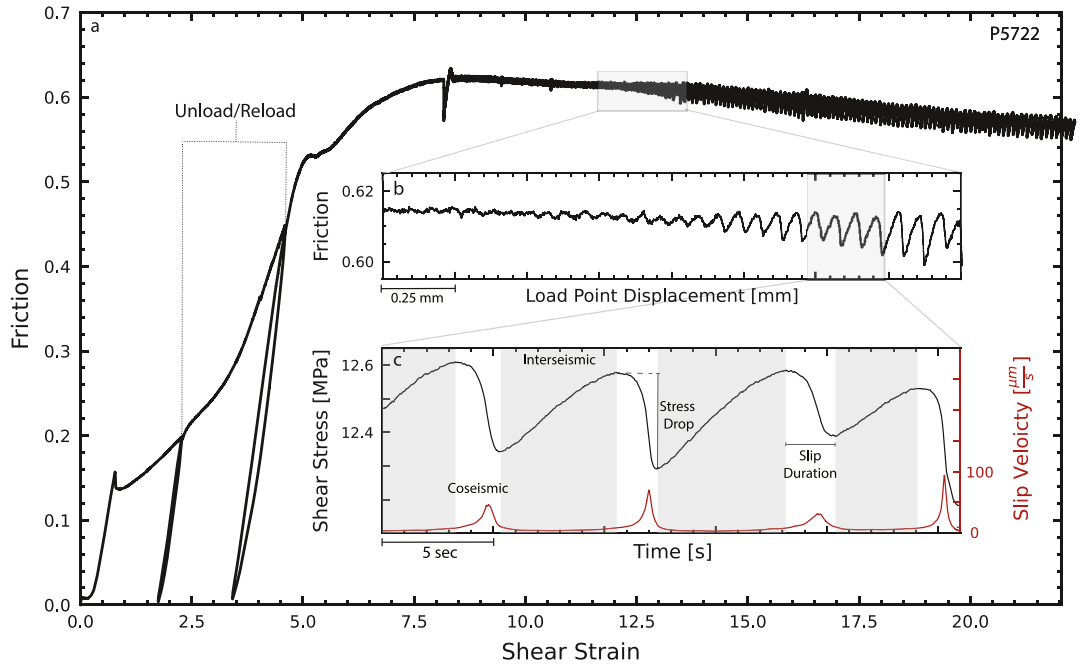

Figure 2. Data for one complete experiment showing fault zone shear stress and shear strain derived from shear displacement and fault thickness. (a) Steady-state friction was reached by shear strains of 7–9. (b) The transitions from stable sliding to slow periodic slips events occurred over a small displacement range and 10–20 seismic cycles. (c) For each stick-slip event, the co- and inter-seismic periods were defined via the shear stress. We measure stress drop, slip duration and slip velocity for each event. Shear loading stiffness was measured from the friction displacement curve during the locked stage of each event (see Figure S3 in Supporting Information S1).

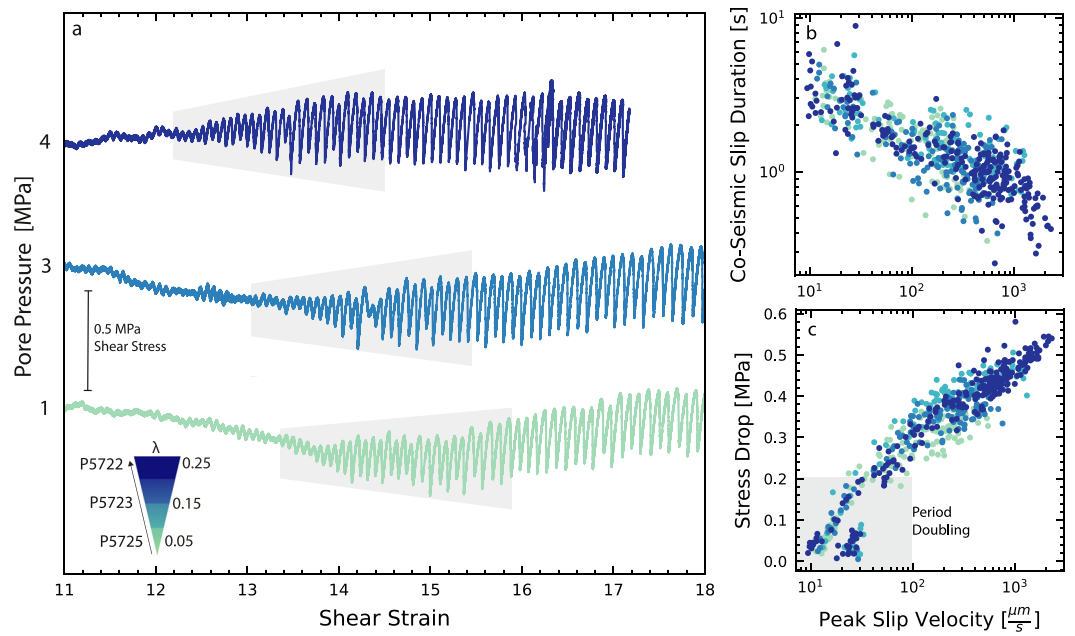

Figure 3. (a) Stick-slip event characteristics for experiments at 3 different pore pressures. Shear stress is plotted versus shear strain during the transition from stable to unstable slip. The transition from small instabilities to quasi-periodic labquakes occurs over a few slip cycles (gray boxes). Panels (b) and (c) show event data for shear strains from 12 to 20 for our complete data set. Stick-slip events evolve from slow to fast, with a log-linear relationship between stress drop and slip velocity. Larger events, with bigger stress drops, reach peak fault slip velocity >1 mm/s with the largest stress drops and corresponding fastest events occurring at the highest λ values. Note the clear trend between co-seismic slip duration and stress drop.

Stress drop was measured as the difference between the maximum shear stress before failure and the minimum shear stress after slip. Stress drops ranged from 0.01 to 0.65 MPa. Slip velocity was calculated using a 0.1 μm displacement-based moving window of the on-fault displacement. Peak slip velocities ranged from just above the background loading rate (10 μm/s) for slow events to 1,100 μm/s for the fastest events. Slip event duration ranged from 0.3 to 7 s. Shear loading stiffness K was measured from (a) unloading/reloading cycles and (b) a linear fit to the shear stress curves during the locked (linear elastic) section of the seismic cycle (see Figure S3 in Supporting Information S1).

3.2. Lab Earthquakes for Faults With Finite Pore Pressure

Our data show a consistent pattern of stable sliding that transitions to creep-slip and stick-slip behavior at shear strains of 10–12 (Figure 3). For our range of conditions, there are minor differences in frictional strength and strain weakening behavior (see Figure S5 in Supporting Information S1), with peak friction coefficient ranging from 0.54 to 0.7. The transition from stable sliding to slow-slip occurs at lower shear strains for higher P_p (Figure 3). However, we do not see a clear correlation between P_p and the strain needed to reach a steady-state limit-cycle, which we define as <10% change in stress drop over a few mm of slip. It is likely that steady-state labquake recurrence times and stress drops are the result of reaching a steady fault zone shear fabric via grain comminution and rearrangement.

The transition from stable sliding to quasi-periodic slow-slip under fluid saturated conditions is quite similar to that observed in previous works without pore fluids (Leeman et al., 2016; Scuderi et al., 2017; Shreedharan et al., 2020). This stage typically has small amplitude modulations in shear stress of 10s of kPa and slip velocity just above background loading velocity. Periods of stable sliding and oscillatory modulation generally occur over the same shear displacement length scales (Figure 3a). There is no apparent correlation between the number of small amplitude modulations and when the fault transitions from stable sliding to quasi-periodic slow-slip. The transition from stable to unstable slip occurs during a period of small amplitude oscillations, and while the inter-seismic period remains near-constant the stress drop magnitude increases over 20–50 events before a steady-state stick-slip cycle is achieved. Over this range, labquake cycles have stress drops <0.2 MPa and slip velocities <100 μm/s. The co-seismic slip duration scales inversely with peak fault slip velocity (Figure 3b). For the stage between stable and unstable slip, the onset of failure is often irregular and difficult to identify, which could explain the data scatter (Figure 3c). As slip events become larger in magnitude and faster, the fault creep rate during the interseismic period decreases systematically (see Figure S6 in Supporting Information S1), matching previous works on the relationship between stress drop and creep rate (Shreedharan et al., 2023). In addition, the co-seismic slip duration decreases during this stage. While friction reaches a quasi-steady state by shear strains of about 15, labquake stress drops continue to grow slowly, increasing from 0.2 to 0.6 MPa with peak slip velocities increasing from 100 to 1,100 μm/s.

3.3. Effect of Loading Stiffness on Fault Stability

For our apparatus and similar machines, the transition from stable to unstable fault slip occurs when loading stiffness K is ≈0.015 MPa/μm (Leeman et al., 2015, 2016; Scuderi et al., 2016; Shreedharan et al., 2020). The effective loading stiffness (apparatus plus fault zone increases initially upon loading as the fault zone compacts but then does not change appreciably after steady-state friction is reached). The onset of slow, quasi-periodic labquakes occurs at a low value of K and evolves over a shear strain of 5–8 (Figure 4). In the context of RSF and fault stability, the transition to unstable motion indicates $K \approx K_c$. The initial stage of unstable motion involves complex slip behaviors including period doubling and aperiodic events. Once steady-state conditions are reached, with more regular labquakes, K then increases at a much slower rate. Consistent with previous work, lower values of K produce larger events with bigger stress drop and higher slip velocity (Leeman et al., 2016; Rudolf et al., 2021), consistent with theory (Gu et al., 1984). Event sizes and magnitudes continue to evolve as a function of strain, with more dynamic events occurring at progressively higher shear strains (Scuderi et al., 2017, 2020).

The stability transition occurs when $K < K_c$, and we observe that both K and K_c evolve with shear strain. We present two estimates for the K_c envelope (Figure 4a). Both thresholds are determined from RSF parameters and a theoretical envelope based on stress dependence of frictional stability (Leeman et al., 2016; Scuderi et al., 2016). The first (dashed red line) assumes minimal rheological evolution, such that K_c is roughly constant with strain, and small changes in K are the cause of event magnitude (Gu et al., 1984; Leeman et al., 2016). Conversely, the second (solid red line) shows a minor evolution of K_c, consistent with lab data (Scuderi et al., 2017). The solid line accounts for small changes in frictional properties and their impact on instability. Because σ_n' is constant,

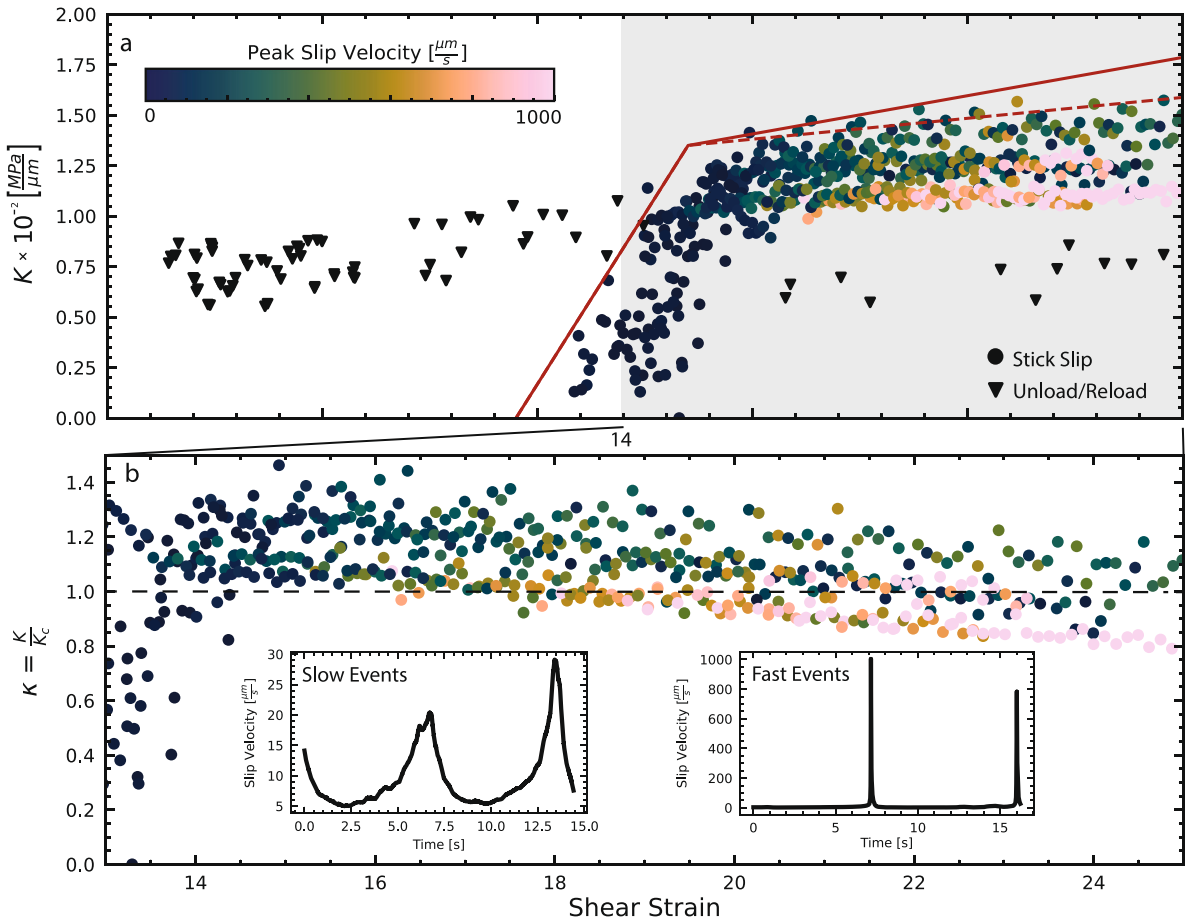

Figure 4. Evolution of the parameters that dictate slip stability with shear strain. Loading stiffness K measured from experiments at 20 MPa σ_n' and P_p from 1 to 4 MPa (Table S1 in Supporting Information S1). (a). Data points show K values measured from unload-reload cycles and stick-slip. Lines show the evolution of K_c with shear strain; the solid line is the preferred model, dashed line shows an alternative model. Note that the transition from stable to unstable slip occurs at a shear strain of ≈14 (see also Figure 1). (b) Zoom of the shaded portion of Panel (a) showing stick-slip evolution from slow to fast slip events, as predicted by theory when data fall below the dashed line showing $\kappa = 1$. Insets shows detail of slip velocity history during slow and fast events at shear strain of 15 and 22, respectively.

K remains nearly constant throughout the experiment, changing only during initial shear when the fault zone compacts and stiffens. Such changes in the effective loading stiffness with strain are linked to densification and shear fabric development. Increases in K_c with strain outpace changes in K. Therefore, once the critical stiffness ratio is reached, with ($\kappa = K/K_c \approx 1$), the evolution of event magnitude is primarily modulated via the rheological stiffness K_c. In accordance with RSF predictions, slow events correspond to κ values from 1.1 to 1.4, whereas faster, more dynamic events typically occur for $\kappa < 1$. The relation between κ and shear strain outpace any effects of λ, such that all experiments follow a similar evolution of labquakes regardless of P_p.

4. Discussion

The pore fluid pressure in a fault zone can affect the mode of sliding via a reduction in σ_n' or via poromechanical effects such as dilatancy strengthening. The key factor could be the absolute value of P_p or the local P_p within the fault zone where changes in pore connectivity dictate the local frictional contact stress. In the context of friction theory, fault strength and the stability transition is determined by σ_n', P_p. and fault permeability. Changes in P_p could produce a change in stability by reducing the effective normal stress, which in isolation promotes slow-slip and stable sliding. Another possibility is that quasi-dynamic changes in fault zone porosity produce either dilatant strengthening or compaction weakening via fluid pressurization (Brantut, 2020; Segall & Rice, 2006; Segall et al., 2010). Our experiments test the assumption that pore fluid pressure is a key factor dictating complex modes of fault slip via dilatancy strengthening or effective normal stress. In one case, P_p drops quashing fault

slip acceleration and in the other, compaction, pore pressure increases and the fault weakens and slips stably. Our experiments explore the requirements for slow-slip with constant P_p boundary conditions and they show that SSE type events can occur even in cases where dilatancy strengthening is negligible. This suggests that SSE on tectonic faults depend as much on frictional rheology as on pore fluids and fault drainage state.

4.1. The Laboratory Seismic Cycle at Constant P_p

Our results agree with the RSF framework for fault stability, and document a transition from stable sliding to unstable slip when loading stiffness $K \approx K_c$, the rheological rate of weakening with slip. The results show that the frictional sliding transition occurs gradually (Figure 2a) over 10–20 laboratory seismic cycles (Figure 3a). P_p has a negligible effect on the loading stiffness K (Figure 4a), suggesting the transition from slow to fast slip is controlled via the rheological stiffness K_c. This conclusion is further reinforced, as event stress drop and slip velocity increases with strain (Figure 4b). This is consistent with theory (Gu et al., 1984) showing that the stability transition is dictated by $\kappa = K/K_c$.

We document a strain-dependent evolution of κ that has two possible mechanisms (Figure 4a). The first, (dashed line) assumes the surrounding medium stiffness K is the driving mechanism. Once the system reaches 'steady-state' event size the characteristics of events dynamics should not change (Leeman et al., 2016; Rudolf et al., 2021). It should be noted, that in a continuum the effective value of K depends on the length of the slipping zone, and controls the critical size of slipping zone in which instabilities occur. Changes in the stiffness of the surrounding medium of the fault could thus modulate the critical stability. In mature fault zones, this is not entirely unlikely, as migrating fluid through the surrounding damage zone would change the stress distribution along the fault. However, we are unable to resolve this assumption as we cannot confidently measure the across-fault porosity contrast under constant pressure boundary condition.

Conversely, the second mechanism (solid line) assumes effective fault stiffness K_c controls the mode of slip. In the second model, we posit that at constant stress conditions when volumetric changes, and thus P_p are sufficiently small, shear fabric evolution is the driving mechanism promoting fault instability. The evolution of spontaneous stick-slips depends on shear fabric evolution (Bedford & Faulkner, 2021; Scuderi et al., 2017, 2020)—assuming the RSF parameters continue to evolve such that K_c outpaces any increase in K through sample compaction and geometric thinning of the gouge. Previous studies have documented the shear strain dependence of the RSF parameters (a, b, Dc) in both synthetic (Den Hartog et al., 2013; Kenigsberg et al., 2020) and natural gouges (den Hartog et al., 2023; Okuda et al., 2023; Shreedharan et al., 2022). These findings may provide insights to fault dynamics as shallow crustal fault cores are often characterized by principal slip planes with cataclasite zones which effectively recycle the material over the slip history. Therefore, we propose that the strain-dependence of the rheological stiffness K_c is the driving mechanism for the stability transition.

At low pore pressures, our results agree with theory and suggest that the effective stress principle predicts the stability transition. In our tests, the contribution from P_p "dead-volume" could mask localized dilational mechanisms, as P_p measurements are not taken directly on the fault (Brantut, 2020). The fault normal permeability decreases from $2.2 * 10^{-17}$ to $8.3 * 10^{-18}$m^2 as a function of shear strain (see Figure S2 in Supporting Information S1). We expect, highly anisotropic permeability within the gouge (Zhang et al., 1999) due to shear fabric mobilization (Niemeijer et al., 2009; Scuderi et al., 2017; Volpe et al., 2022). Given the K_c increases with strain, we would expect that lower permeability would amplify any localized Pp effects—possibly influencing the frictional parameters. However, we observe negligible changes in stress drop, slip velocity or co-seismic slip duration (Figures 3b and 3c) in response to Pp. We cannot rule out the role of P_p in natural fault systems, but it seems possible that slow-slip events are caused by more than just the presence of elevated pore pressures. To activate the dilational mechanisms invoked for SSEs, we believe specific attention needs to be given to the fault drainage state throughout the seismic cycle (Perez-Silva et al., 2023).

4.2. Fault Drainage State and Frictional Stability

Under constant pressure boundary conditions, the stress dependence of RSF parameters (a, b, D_c) depend on fault zone volume changes via dilation/compaction and the fluid diffusion time. Recent friction studies at higher pore pressure and studies of intact fractures show that fault dilation can result in significant P_p transients (Aben & Brantut, 2021; Brantut, 2020; Proctor et al., 2020). These experiments documented undrained conditions and local reduction of P_p. We evaluated the possibility that our experiments also involved undrained loading due to co-seismic slip. We did this by comparing pore fluid volume changes with changes in layer thickness, following previous

work (Samuelson et al., 2009). This comparison shows that our loading conditions were drained (see Figure S2 in Supporting Information S1), suggesting that pore fluid did not change locally during inter-seismic cycles.

In other works, the evolution of fault zone permeability has been related to changes in porosity (Crawford et al., 2008; Faulkner et al., 2018) due to grain size reduction during shearing (Bedford & Faulkner, 2021; Collettini et al., 2011; Niemeijer et al., 2010). These works further suggest an increase in the complexity of the fluid pathways due to shear fabric evolution (Zhang et al., 1999). In this case, the characteristic drainage time due to the internal generation of pore fluid pressures is,

$$t = \frac{L^2 \mu * (\beta_p + \Phi \beta_w)}{2k} \quad (2)$$

where L is layer thickness over the duration of shearing (900–2,100 μm), μ is dynamic viscosity of water ($0.89 * 10^{-3}$ Pa s), ϕ is porosity before and after shearing (0.04–0.12), k is permeability ($8.3 * 10^{-18}$ to $2.2 * 10^{-17}$ m^2) and β_p ($1.1 - 2.5 * 10^{-8}$ Pa^{-1}) and β_w ($4.6 * 10^{-10}$ Pa^{-1}) are the compressibility of the porous medium and fluid. For our experiments, Equation 2 gives a fluid diffusion time ranging from 0.89 to 1.08 s, which is consistent with our measurements of porosity and layer thickness change (see Text S2 and Figure S7 in Supporting Information S1). Thus, peak slip velocities of 1,100 μm/s could sustain localized over-pressure or under-pressure—effectively weakening, or strengthening the fault. Within this framework, shear-induced changes in P_p are controlled by changes in fault volume and the duration of these effects would increase as permeability decreases. Therefore, at the same loading velocity, the permeability-shear strain evolution is the primary mechanism controlling P_p—slip responses. Critical to our study is the observation that local changes in P_p have a minor impact on fault zone friction throughout the seismic cycle, yet we observe the complete spectrum of slip behaviors from creep to slow slip and dynamic rupture.

Importantly, our study demonstrates that at low P_p, despite the fault hosting instances of slightly undrained fluid pressure, there is no resolvable effect on fault slip or stress drop. When fluid effects are important, fault weakening or strengthening can be rate-controlled by fluid diffusion (Paola et al., 2007; Perez-Silva et al., 2023). The fault plane will experience periodic increased or decreased frictional strength based on the sense of porosity change (Segall et al., 2010; Sibson, 1986)—whether compactive or dilational. We find that the short pore pressure diffusion time across the fault relative to the inter-seismic duration causes any local stress change to be erased before the next event occurs. Our results demonstrate that across low P_p conditions frictional processes alone are sufficient to explain stick-slip evolution. We note that the spectrum of complex slip phenomena observed in nature may be dictated more by frictional rheology than by pore fluid pressures.

5. Conclusion

We conducted friction experiments on synthetic quartz gouge across a range of pore fluid pressures at constant fluid pressure boundary conditions. We document the full transition from quasi-dynamic slow slip to periodic elastodynamic stick-slip as a function of the rheological weakening rate of the fault K_c. We test the hypothesis that slow-slip is caused by changes in fluid pressure and dilatancy strengthening associated with the fault drainage state. Our results indicate that for low pore pressures with fluid diffusion times less than the inter-seismic duration, slow-slip events can occur entirely from strain rate dependence of frictional rheology, dictated by K_c. Our results corroborate the finding that frictional evolution evolves from shear fabric mobilization and suggests that special attention should be given to how such shear fabrics interact with the hydromechanical properties of fault zones. Our findings highlight the importance of studies that connect the frictional evolution, fault drainage state, and effective normal stress dependence of poro-mechanical processes controlling fault evolution.

Data Availability Statement

All data sets collected during the study are available on Zenodo (Affinito et al., 2023, https://doi.org/10.5281/zenodo.7734607).

Acknowledgments
We thank Steven Swavely for laboratory technical support and Drs. Srisharan Shreedharan, David (Chas) Bolton, Marco Scuderi, Carolina Giorgetti and Aagje Eijsink for scientific support and discussions. We thank Drs. Ernest Rutter and John W. Rudnicki for constructive comments. This work was supported by US Department of Energy Grants DE-SC0020512 and DE-EE0008763. Chris Marone also acknowledges support from European Research Council Advance Grant 835012 (TECTONIC) and Partenariato Esteso RETURN, finanziato dall'Unione Europea—NextGenerationEU (Piano Nazionale di Ripresa e Resilienza—PNRR, Missione 4 Componente 2, Investimento 1.3—D.D. 1243 2/8/2022, PE0000005; Spoke VS3).

References

Aben, F., & Brantut, N. (2021). Dilatancy stabilises shear failure in rock. *Earth and Planetary Science Letters*, *574*, 1–34. https://doi.org/10.1016/j.epsl.2021.117174

Affinito, R., Wood, C., Marty, S., Elsworth, D., & Marone, C. (2023). The stability transition from stable to unstable frictional slip with finite pore pressure [Dataset]. Geophysical Research Letters. Zenodo. https://doi.org/10.5281/zenodo.7734607

Bedford, J. D., & Faulkner, D. R. (2021). The role of grain size and effective normal stress on localization and the frictional stability of simulated quartz gouge. *Geophysical Research Letters*, *48*(7), e2020GL092023. https://doi.org/10.1029/2020gl092023

Behr, W., & Bürgmann, R. (2021). What's down there? The structures, materials and environment of deep-seated slow slip and tremor. *Philosophical Transactions of the Royal Society A: Mathematical, Physical & Engineering Sciences*, *379*(2193), 20200218. https://doi.org/10.1098/rsta.2020.0218

Brantut, N. (2020). Dilatancy-induced fluid pressure drop during dynamic rupture: Direct experimental evidence and consequences for earthquake dynamics. *Earth and Planetary Science Letters*, *538*, 1–25. https://doi.org/10.1016/j.epsl.2020.116179

Bürgmann, R. (2018). The geophysics, geology and mechanics of slow fault slip. *Earth and Planetary Science Letters*, *495*, 112–134. https://doi.org/10.1016/j.epsl.2018.04.062

Collettini, C., Niemeijer, A., Viti, C., Smith, S., & Marone, C. (2011). Fault structure, frictional properties and mixed-mode fault slip behavior. *Earth and Planetary Science Letters*, *311*(3–4), 316–327. https://doi.org/10.1016/j.epsl.2011.09.020

Condit, C., & French, M. (2022). Geologic evidence of lithostatic pore fluid pressures at the base of the subduction seismogenic zone. *Geophysical Research Letters*, *49*(12), e2022GL098862. https://doi.org/10.1029/2022gl098862

Crawford, B., Faulkner, D., & Rutter, E. (2008). Strength, porosity, and permeability development during hydrostatic and shear loading of synthetic quartz-clay fault gouge. *Journal of Geophysical Research*, *113*(B3), B03207. https://doi.org/10.1029/2006jb004634

Dal Zilio, L., Lapusta, N., & Avouac, J.-P. (2020). Unraveling scaling properties of slow-slip events. *Geophysical Research Letters*, *47*(10), e2020GL087477. https://doi.org/10.1029/2020gl087477

den Hartog, S., Marone, C., & Saffer, D. (2023). Frictional behavior downdip along the subduction megathrust: Insights from laboratory experiments on exhumed samples at in situ conditions. *Journal of Geophysical Research: Solid Earth*, *128*(1), e2022JB024435. https://doi.org/10.1029/2022jb024435

Den Hartog, S., Niemeijer, A., & Spiers, C. (2013). Friction on subduction megathrust faults: Beyond the illite–muscovite transition. *Earth and Planetary Science Letters*, *373*, 8–19. https://doi.org/10.1016/j.epsl.2013.04.036

Dieterich, J. (1979). Modeling of rock friction 1. experimental results and constitutive equations. *Journal of Geophysical Research*, *84*(B5), 2161–2168. https://doi.org/10.1029/JB084iB05p02161

Ellsworth, W. (2013). Injection-induced earthquakes. *Science*, *341*(6142), 1225942. https://doi.org/10.1126/science.1225942

Faulkner, D., & Rutter, E. (2001). Can the maintenance of overpressured fluids in large strike-slip fault zones explain their apparent weakness? *Geology*, *29*(6), 503–506. https://doi.org/10.1130/0091-7613(2001)029<0503:ctmoof>2.0.co;2

Faulkner, D., Sanchez-Roa, C., Boulton, C., & Den Hartog, S. (2018). Pore fluid pressure development in compacting fault gouge in theory, experiments, and nature. *Journal of Geophysical Research: Solid Earth*, *123*(1), 226–241. https://doi.org/10.1002/2017jb015130

Gu, J., Rice, J., Ruina, A., & Tse, S. (1984). Slip motion and stability of a single degree of freedom elastic system with rate and state dependent friction. *Journal of the Mechanics and Physics of Solids*, *32*(3), 167–196. https://doi.org/10.1016/0022-5096(84)90007-3

Hubbert, K., & Rubey, W. (1959). Role of fluid pressure in mechanics of overthrust faulting: I. Mechanics of fluid-filled porous solids and its application to overthrust faulting. *GSA Bulletin*, *70*(2), 115–166. https://doi.org/10.1130/0016-7606(1959)70[115:ROFPIM]2.0.CO;2

Ikari, M., Saffer, D., & Marone, C. (2009). Frictional and hydrologic properties of clay-rich fault gouge. *Journal of Geophysical Research*, *114*(B5), B05409. https://doi.org/10.1029/2008JB006089

Ji, Y., Hofmann, H., Rutter, E., & Zang, A. (2022). Transition from slow to fast injection-induced slip of an experimental fault in granite promoted by elevated temperature. *Geophysical Research Letters*, *49*(23), e2022GL101212. https://doi.org/10.1029/2022gl101212

Kenigsberg, A., Rivière, J., Marone, C., & Saffer, D. (2020). Evolution of elastic and mechanical properties during fault shear: The roles of clay content, fabric development, and porosity. *Journal of Geophysical Research: Solid Earth*, *125*(3), 1–16. https://doi.org/10.1029/2019JB018612

Leeman, J., Saffer, D., Scuderi, M., & Marone, C. (2016). Laboratory observations of slow earthquakes and the spectrum of tectonic fault slip modes. *Nature Communications*, *7*, 1–6. https://doi.org/10.1038/ncomms11104

Leeman, J., Scuderi, M., Marone, C., & Saffer, D. (2015). Stiffness evolution of granular layers and the origin of repetitive, slow, stick-slip frictional sliding. *Granular Matter*, *17*(4), 447–457. https://doi.org/10.1007/s10035-015-0565-1

Marone, C. (1998). Laboratory-derived friction laws and their application to seismic faulting. *Annual Review of Earth and Planetary Sciences*, *26*(1), 643–696. https://doi.org/10.1146/annurev.earth.26.1.643

Marone, C., Raleigh, C., & Scholz, C. (1990). Frictional behavior and constitutive modeling of simulated fault gouge. *Journal of Geophysical Research*, *95*(B5), 7007–7025. https://doi.org/10.1029/JB095iB05p07007

Niemeijer, A., Elsworth, D., & Marone, C. (2009). Significant effect of grain size distribution on compaction rates in granular aggregates. *Earth and Planetary Science Letters*, *284*(3–4), 386–391. https://doi.org/10.1016/j.epsl.2009.04.041

Niemeijer, A., Marone, C., & Elsworth, D. (2010). Frictional strength and strain weakening in simulated fault gouge: Competition between geometrical weakening and chemical strengthening. *Journal of Geophysical Research*, *115*(10), 1–16. https://doi.org/10.1029/2009JB000838

Okuda, H., Niemeijer, A. R., Takahashi, M., Yamaguchi, A., & Spiers, C. J. (2023). Hydrothermal friction experiments on simulated basaltic fault gouge and implications for megathrust earthquakes. *Journal of Geophysical Research: Solid Earth*, *128*(1), e2022JB025072. https://doi.org/10.1029/2022jb025072

Paola, N. D., Collettini, C., Trippetta, F., Barchi, M. R., & Minelli, G. (2007). A mechanical model for complex fault patterns induced by evaporite dehydration and cyclic changes in fluid pressure. *Journal of Structural Geology*, *29*(10), 1573–1584. https://doi.org/10.1016/j.jsg.2007.07.015

Perez-Silva, A., Kaneko, Y., Savage, M., Wallace, L., & Warren-Smith, E. (2023). Characteristics of slow slip events explained by rate-strengthening faults subject to periodic pore fluid pressure changes. *Journal of Geophysical Research: Solid Earth*, *128*(6), e2022JB026332. https://doi.org/10.1029/2022jb026332

Proctor, B., Lockner, D., Kilgore, B., Mitchell, T., & Beeler, N. (2020). Direct evidence for fluid pressure, dilatancy, and compaction affecting slip in isolated faults. *Geophysical Research Letters*, *47*(16), e2019GL086767. https://doi.org/10.1029/2019GL086767

Rice, J. (2006). Heating and weakening of faults during earthquake slip. *Journal of Geophysical Research*, *111*(B5), B05311. https://doi.org/10.1029/2005JB004006

Rudolf, M., Rosenau, M., & Oncken, O. (2021). The spectrum of slip behaviors of a granular fault gouge analogue governed by rate and state friction. *Geochemistry, Geophysics, Geosystems*, *22*(12), e2021GC009825. https://doi.org/10.1029/2021gc009825

Ruina, A. (1983). Slip instability and state variable friction laws. *Journal of Geophysical Research*, *88*(B12), 10359–10370. https://doi.org/10.1029/JB088iB12p10359

Sacks, I. S., Linde, A. T., Suyehiro, S., & Snoke, J. A. (1978). Slow earthquakes and stress redistribution. *Nature*, *275*(5681), 599–602. https://doi.org/10.1038/275599a0

Samuelson, J., Elsworth, D., & Marone, C. (2009). Shear-induced dilatancy of fluid-saturated faults: Experiment and theory. *Journal of Geophysical Research*, *114*(12), 1–15. https://doi.org/10.1029/2008JB006273

Scuderi, M., Collettini, C., Vitti, C., Tinti, E., & Marone, C. (2017). Evolution of shear fabric in granular fault gouge from stable sliding to stick slip and implications for fault slip mode. *Geology*, *45*(8), 731–734. https://doi.org/10.1130/G39033.1

Scuderi, M., Marone, C., Tinti, E., Di Stefano, G., & Collettini, C. (2016). Precursory changes in seismic velocity for the spectrum of earthquake failure modes. *Nature Geoscience*, *9*(9), 695–700. https://doi.org/10.1038/ngeo2775

Scuderi, M., Tinti, E., Cocco, M., & Collettini, C. (2020). The role of shear fabric in controlling breakdown processes during laboratory slow-slip events. *Journal of Geophysical Research: Solid Earth*, *125*(11), e2020JB020405. https://doi.org/10.1029/2020jb020405

Segall, P., & Rice, J. (2006). Does shear heating of pore fluid contribute to earthquake nucleation? *Journal of Geophysical Research*, *111*(B9), B09316. https://doi.org/10.1029/2005jb004129

Segall, P., Rubin, A., Bradley, A., & Rice, J. (2010). Dilatant strengthening as a mechanism for slow slip events. *Journal of Geophysical Research*, *115*(12), 1–37. https://doi.org/10.1029/2010JB007449

Shreedharan, S., Bolton, D., Rivière, J., & Marone, C. (2020). Preseismic fault creep and elastic wave amplitude precursors scale with lab earthquake magnitude for the continuum of tectonic failure modes. *Geophysical Research Letters*, *47*(8), 1–10. https://doi.org/10.1029/2020GL086986

Shreedharan, S., Ikari, M., Wood, C., Saffer, D., Wallace, L., & Marone, C. (2022). Frictional and lithological controls on shallow slow slip at the northern Hikurangi margin. *Geochemistry, Geophysics, Geosystems*, *23*(2), e2021GC010107. https://doi.org/10.1029/2021gc010107

Shreedharan, S., Saffer, D., Wallace, L., & Williams, C. (2023). Ultralow frictional healing explains recurring slow slip events. *Science*, *379*(6633), 712–717. https://doi.org/10.1126/science.adf4930

Sibson, R. (1986). Earthquakes and rock deformation in crustal fault zones. *Annual Review of Earth and Planetary Sciences*, *14*(1), 149–175. https://doi.org/10.1146/annurev.ea.14.050186.001053

Volpe, G., Pozzi, G., & Collettini, C. (2022). YBPR or SCC? Suggestion for the nomenclature of experimental brittle fault fabric in phyllosilicate-granular mixtures. *Journal of Structural Geology*, *165*, 104743. https://doi.org/10.1016/j.jsg.2022.104743

Wibberley, C. (2002). Hydraulic diffusivity of fault gouge zones and implications for thermal pressurization during seismic slip. *Earth Planets and Space*, *54*(11), 1153–1171. https://doi.org/10.1186/BF03353317

Williams, R. (2019). Coseismic boiling cannot seal faults: Implications for the seismic cycle. *Geology*, *47*(5), 461–464. https://doi.org/10.1130/G45936.1

Zhang, S., Tullis, T., & Scruggs, V. (1999). Permeability anisotropy and pressure dependency of permeability in experimentally sheared gouge materials. *Journal of Structural Geology*, *21*(7), 795–806. https://doi.org/10.1016/s0191-8141(99)00080-2